Journal of
Instrumentation



# A scintillator veto detector prototype for low energy charged beam particles



Published by IOP Publishing for Sissa Medialab

Received: *May 20, 2025*
Accepted: *July 17, 2025*
Published: *August 26, 2025*

International workshop on
Detection Systems and Techniques for fundamental and applied physics
Catania, Italy
24–26 February 2025

# A scintillator veto detector prototype for low energy charged beam particles

**M.G. Pellegriti,**[a,*] **S. Boscarino,**[b] **I. Lombardo,**[a,b] **A. Musumarra,**[a,b] **G. Pellegrino,**[c] **T. Roger**[d] **and F. Ruffino**[b,c]

[a] *Istituto Nazionale di Fisica Nucleare (INFN), Sezione di Catania, Via Santa Sofia 64, 95123 Catania, Italy*
[b] *Dipartimento di Fisica e Astronomia, Università di Catania, Via Santa Sofia 64, 95123 Catania, Italy*
[c] *Consiglio Nazionale delle Ricerche, Istituto per la Microelettronica e Microsistemi (CNR-IMM), Via Santa Sofia 64, 95123 Catania, Italy*
[d] *Grand Accélérateur National d'Ions Lourds (GANIL), Bvd Henri Becquerel, 14076 Caen, France*

*E-mail:* mariagrazia.pellegriti@ct.infn.it

Abstract: A detector prototype developed as a fast veto system for low-energy charged particles, designed to operate in a gaseous active target environment (Time Projection chamber, TPC) is presented. The detector employs a fast plastic scintillator optically coupled to a silicon photomultiplier (SiPM) through a light guide, enabling the relocation of the SiPM outside the active volume of the TPC.

To enhance sensitivity to low-energy particles while minimizing energy losses, which is a general issue in the use of scintillators for charged particle detection, a thin platinum layer was deposited via a sputtering technique on the scintillator front surface. This layer acts, at the same time, as a light-tight window and as a reflective surface for the scintillation light produced within the active volume.

This study, in particular, focuses on the use of NE-102A plastic scintillators ($20 \times 20\,\mathrm{mm}^2$, 3.2 mm thick) with a deposited platinum coatings ranging from 34 nm to 68 nm for the detection of low-energy light charged particles. Preliminary tests by using $3 \times 3\,\mathrm{mm}^2$ SiPMs show a linear light response and an energy resolution comparable to those obtained by using standard aluminized Mylar windows. Further developments include coupling the scintillators with larger-area SiPMs ($6 \times 6\,\mathrm{mm}^2$) to further increase light collection efficiency, lower the energy threshold and improve energy resolution.

The results of the prototype's characterization and functional testing are presented, along with an outlook on future improvements and applications.

Keywords: Scintillators and scintillating fibres and light guides; Very low-energy charged particle detectors

*Corresponding author.



https://doi.org/10.1088/1748-0221/20/08/C08021

2025 JINST 20 C08021

## Contents


1 **Detector development: motivations and structure** 1

2 **Platinum layer: deposition and characterization** 2

3 **Prototype assemblies and calibrations** 4

4 **Conclusions and perspectives** 6




## 1 Detector development: motivations and structure

The research environment for the present prototype detector development is grounded on the proposal for a new $^{8}$Li($\alpha$,n)$^{11}$B cross-section determination [1], aiming at solving the discrepancy between existing experimental data at the astrophysical relevant energies [2]. The proposed experimental set-up is merging the use of the thick target inverse kinematics (TTIK) method [3] with the use of the high tracking performances and vertex reconstruction of ACtive TARget and Time Projection Chamber (ACTAR TPC) [4]. The TTIK allows to obtain the cross section in a wide $\alpha$-$^{8}$Li center-of-mass energy range by using the beam energy losses in the gas target while the ACTAR TPC is devoted to the detection of the $^{11}$B ejectile, precisely determining the center-of-mass energy by vertex discrimination. The non-interacting $^{8}$Li beam particles, which reach the end of the ACTAR active region at low energy (< 1 MeV), are planned to be detected in a beam dump veto detector (a 500 µm four quadrant silicon detector) such as to be excluded from the main acquisition trigger.

The detector prototype described in this paper has been developed as an alternative to the previously mentioned silicon veto detector. It is divided into four sectors, each comprising a scintillator foil covered by a very thin window layer, and optically coupled to a square SiPM sensor via a truncated square pyramid light guide, see figure 1.

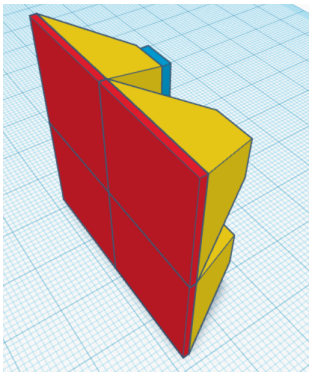

**Figure 1.** Detector set-up: each sector consists of a scintillator foil (red) covered by a very thin layer window and coupled through a truncated square pyramid light-guide (yellow) to a square SiPM sensor (cyan).

Eljen EJ-212 [5] was selected as the scintillator material. It is a fast plastic scintillator based on polyvinyltoluene, designed for the detection of beta particles and other charged particles. It offers high light output (approximately 64% of anthracene), a fast rise time of about 0.9 ns, a 2.7 ns FWHM pulse width and an emission peak around 423 nm. Its mechanical stability and ease of machining make it suitable for thin-film applications, including layers as thin as 1 mm. EJ-212 is non-hygroscopic and vacuum compatible, has a density of roughly 1.023 g/cm$^3$, and a refractive index of 1.58. It is commercially equivalent to Bicron BC-400 and NE-102A, with similar optical and physical properties. For the initial prototype tests, three NE-102A scintillators were used, each with a surface area of 20 $\times$ 20 mm$^2$ and a thickness of 3.2 mm. The Hamamatsu MPPC SiPM [7] were chosen, in particular the S13360-3050CS (3 $\times$ 3 mm$^2$) for test purposes and the S13360-6050CS (6 $\times$ 6 mm$^2$) for the final assembly. They are solid-state photon detectors with high photon detection efficiency and fast response and operate around 54–58 V bias. Four 70 mm long truncated square pyramid light-guide made of PMMA [6], with input and output surfaces of 20 $\times$ 20 mm$^2$ and 3 $\times$ 3 mm$^2$, are expected to be used in the final set-up to optically couple the scintillators to the SiPM sensors, enabling the relocation of the SiPM outside the active volume of the TPC. For the preliminary tests described in this paper 3 $\times$ 3 mm$^2$ SiPMs were directly coupled to the NE-102A samples.

## 2 Platinum layer: deposition and characterization

To allow a light-tight operation of the scintillator and to increase the internal light collection by improving the window inner reflectance, while minimizing energy loss from low-energy charged particles, is a general issue for scintillators. In the present case, a thin layer of platinum was deposited on the scintillator surface by using a sputtering technique. Preliminary simulations were carried out using the SRIM software [11] to determine the optimal thickness of the platinum layer. Specifically, energy loss simulations for a 50 nm Pt layer were performed with a 300 keV $^8$Li beam, resulting in an energy loss of approximately 30 keV and a full width at half maximum (FWHM) of 26 keV. During the detector development phase, the platinum deposition procedure was tested on NE-102A samples.

Very thin platinum layers, with thicknesses ranging from 34 nm to 68 nm, were deposited on the scintillator front surfaces using the Emitech K550X RF sputter coater from Dipartimento di Fisica e Astronomia, University of Catania. This compact benchtop system, equipped with a DC source, is well-suited for a rapid and uniform metal layer deposition. Specifically, by using a current of 50 mA and deposition times of 480 s, 417 s and 240 s, measured thicknesses for the Pt layer of 68 $\pm$ 5 nm, 55 $\pm$ 5 nm and 34 $\pm$ 5 nm were obtained. Thickness measurements were carried out by using a silicon wafer placed alongside the scintillator during the deposition process. The wafer was later sectioned and analyzed by scanning electron microscopy (SEM), at DFA, University of Catania. SEM surface and cross-sectional inspections for the 34 nm and 55 nm layers are presented in figure 2. Sheet resistance measurements were performed on the same samples by using the Van der Pauw method, yielding values of 46 $\Omega$/sq and 35 $\Omega$/sq, respectively. These results imply that both surfaces are conductive. Transmission characterization of the two plastic scintillator samples before and after the Pt deposit layer of 55 nm and 34 nm, obtaining 3% and 7% transmittance respectively for the scintillator light spectral range (see figure 3), thus allowing a good reflection for the light produced inside the scintillator by the detected particles.



2025 JINST 20 C08021

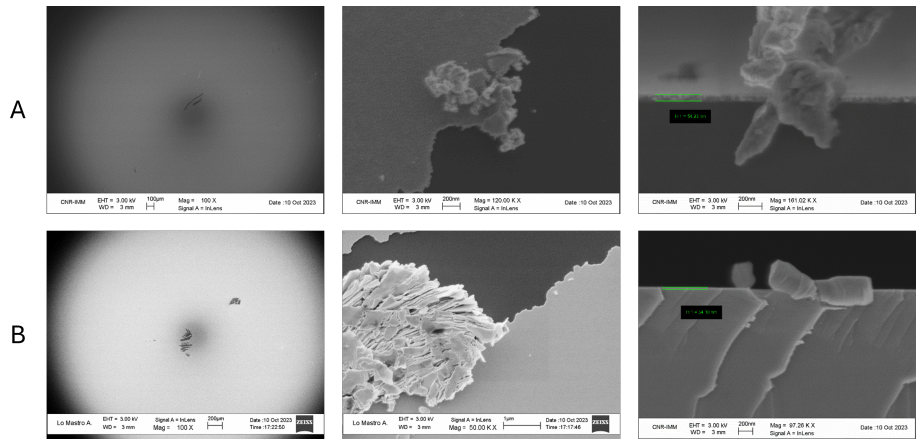


**Figure 2.** Scanning electron microscope (SEM) images of two different Pt layer deposits (A and B) obtained by using two different deposition times in the sputtering source: 417 s (A) and 240 s (B). In the left and middle column a surface inspection at two different magnification (100 and 50 k). In the right column, the cross section of a silicon wafer, placed alongside the scintillator to allow the thickness measurement of the two layers, respectively 55 ± 5 nm (A) and 34 nm ± 5 nm (B).

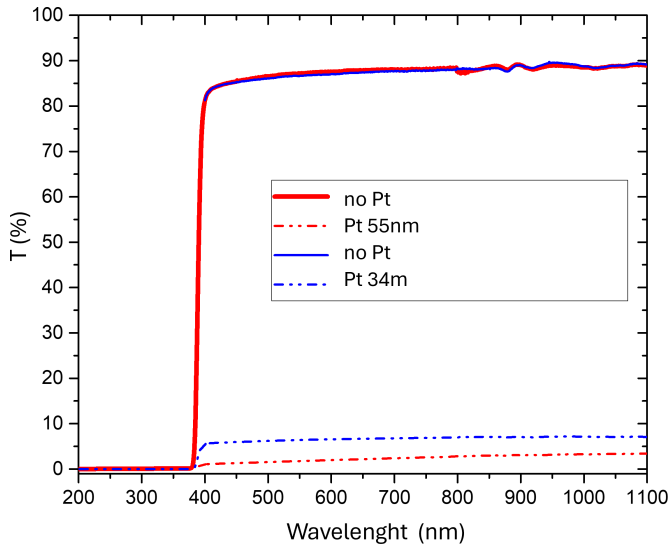


**Figure 3.** Transmission characterization of the two plastic scintillator samples before (solid lines) and after the Pt deposit layer of 55 nm and 34 nm (dashed lines).

Near-infrared (NIR) transmission characterization for the scintillator samples before and after the 55 nm and 34 nm Pt layer deposit were also performed (see figure 4). The resonance structures of polyvinyltoluene were observed in all cases, indicating that the sputtering process (including sample heating) did not significantly alter the scintillator's structure. NIR transmittance in the Pt-coated samples was also reduced on average by the same factor observed in visible-range transmittance, due to the attenuating effect of the platinum overlayer.



2025 JINST 20 C08021

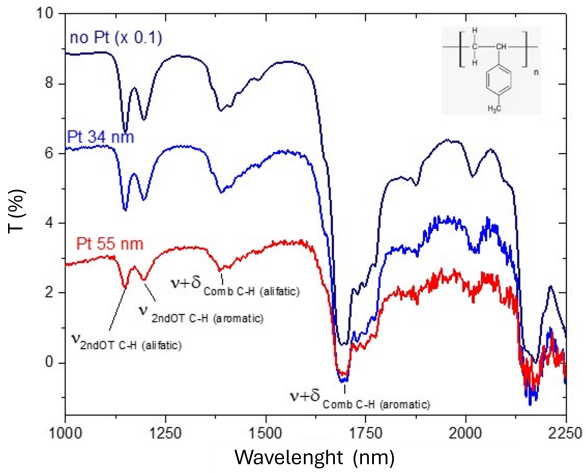


**Figure 4.** NIR transmittance spectra related to the scintillator before (black curve) and after the deposition of 34 nm (blue curve) and 55 nm (red curve) Pt layers. The spectra show the overtone (OT) and combination (Comb) bands associated with polyvinyltoluene vibrational modes.

## 3 Prototype assemblies and calibrations

Three sensors were then assembled by using two different Pt layer thickness 34 ± 5 nm and 55 ± 5 nm and a 2 ± 0.03 µm aluminized mylar window (40 ± 0.7 nm Al coating). The back surfaces of the three scintillators were then optically coupled to 3 × 3 $mm^2$ S13360-3050CS SiPM from Hamamatsu by using optical grease. The sensor holders were obtained by using a 3D printer with a PLA filament (1.75 mm thick). The inner surface of the holder was covered with a white Teflon tape layer to increase light reflection from the scintillator's back surface and thus enhance SiPM light collection. The assembling procedure, for one of the Pt layer deposited samples, is shown in figure 5.

The cathode and anode of the SiPM were then connected to a custom readout circuit, designed to simultaneously enable biasing and signal extraction. The bias voltage was supplied by using a CAEN A7585DU SiPM Power Module [8], while the output signal was amplified by a Nooelec HF LaNa ultra-low-noise HF amplifier [9]. Signals were processed by using a table top CAEN DT5743 digitizer [10].

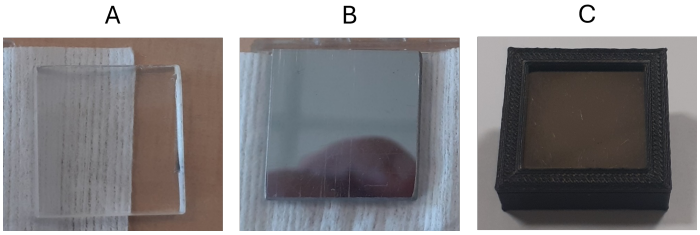


**Figure 5.** A 20 × 20 $mm^2$ bare scintillator and a Platinum layer deposited one are shown respectively in A and B. A complete Pt deposited prototype sensor is shown inside its holder in C.

In-vacuum characterization was performed by using a collimated $^{241}$Am $\alpha$-source (5.486 MeV) (see figure 6). The $\alpha$ particle energy losses, for this incoming energy, are 16 keV, 25 keV, and 231 keV for the 34 nm Pt layer window, 55 nm Pt layer window, and 2 µm aluminized mylar window, respectively.



2025 JINST 20 C08021

The charge signal, obtained from the analysis of the digitizer waveforms, is shown for the three sensors in figure 6 (left). It was observed that the sensor equipped with an aluminized Mylar window exhibited a higher light collection efficiency compared to the sensors with a platinum-coated window. Among the latter, the sensor with the thicker platinum layer showed a reduced light collection performance. A possible explanation for this result might be the longer exposure time at 50°C in the sputtering source oven, though further investigation would be needed to confirm this hypothesis.

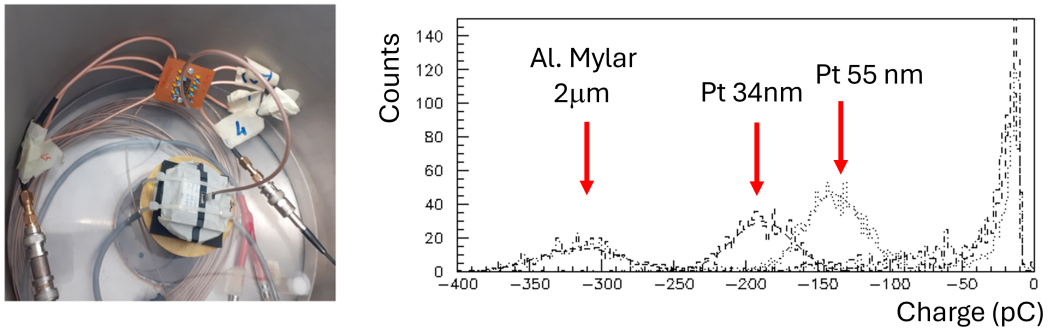


**Figure 6.** A picture of the $^{241}$Am $\alpha$-source set-up inside the vacuum chamber (left side). The $\alpha$ particles spectrum measured by using the three sensors (right side); the obtained spectra for the three different assembled sensors have been superimposed in the plot.

At this stage, the sensor with the 34 nm Pt layer window and the one with the aluminized Mylar window were further characterized to estimate their detection energy thresholds for alpha particles. This characterization was performed by using an energy calibration with the $^{241}$Am $\alpha$-source in two additional configurations, compared to the one previously used, employing two sets of energy degraders (see figure 7). The results of the energy loss simulations for the three source configurations and for both sensors are reported in the table 1. The uncertainties in the reported energy values were estimated by quadratically adding two contributions: (i) the error due to energy straggling, simulated with SRIM using the nominal layer thicknesses, and (ii) the error from energy variation arising from thickness uncertainties. Mean energies were independently calculated as a cross-check with the LISE$^{++}_{\text{cute}}$ physical calculator (ATIMA energy-loss model) [12]. These mean values agree, within the error bars, with the SRIM simulations listed in table 1. The corresponding charge signal analyses and the outcomes of the two calibrations are shown in the figure 8. From the analysis of the calibration curves, a linear response was observed in both cases, with a comparable energy resolution of approximately 18%. The extrapolated energy threshold was 1.86 ± 0.07 MeV for the sensor with the 34 nm Pt layer and 1.11 ± 0.09 MeV for the one with the aluminized Mylar window.

**Table 1.** Calibration energies for the two sensors, evaluated by using SRIM energy loss software considering the initial 5.486 MeV $^{241}$Am $\alpha$-source energy, in the three calibration configurations of figure 7. Calculation includes also the energy loss in the two sensor windows.

| Calibration set-up | 1 | 2 | 3 |
|---|---|---|---|
| | $E \pm \Delta E$ (MeV) | $E \pm \Delta E$ (MeV) | $E \pm \Delta E$ (MeV) |
| sensor window: Pt 34 nm | 5.470 ± 0.004 | 3.529 ± 0.053 | 2.709 ± 0.076 |
| sensor window: Al Mylar 2um | 5.255 ± 0.010 | 3.235 ± 0.068 | 2.358 ± 0.085 |



2025 JINST 20 C08021

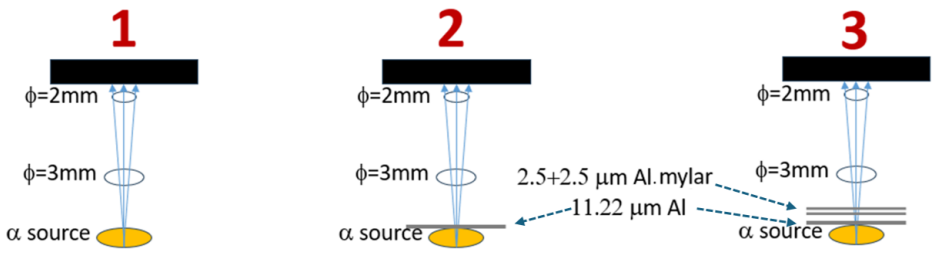


**Figure 7.** Calibration setup. The first configuration consists of a collimated $^{241}$Am $\alpha$-source irradiating the sample. The second configuration includes an 11.22 ± 0.19 µm aluminum foil acting as an energy degrader for the $\alpha$ particles. The third configuration combines the same aluminum foil with two additional aluminized mylar foils, each 2.5 µm thick, with a total 5.00 ± 0.06 µm mylar thickness and 80 ± 1 nm Al coating thickness.

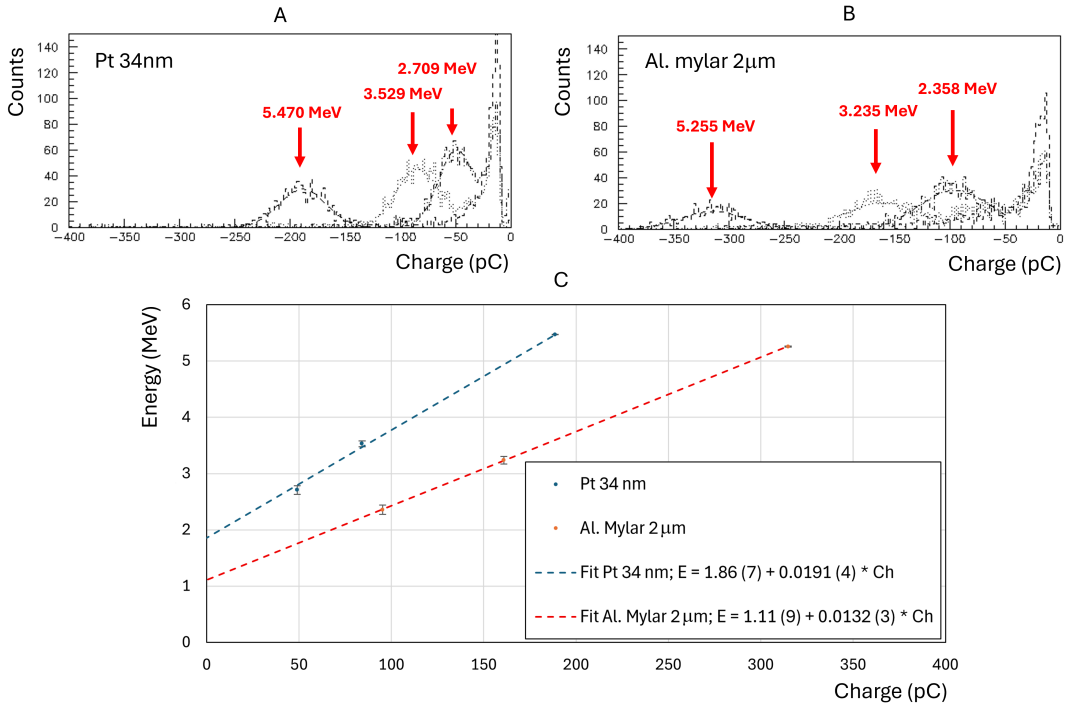


**Figure 8.** Alpha particles spectra measured by using three different energies (see table 1) by the two sensors (A and B) have been superimposed in the plot. In C, the energy calibration curve obtained for the two cases.

## 4 Conclusions and perspectives

In this work we performed a feasibility study concerning the use of thin plastic scintillators coated with platinum layers ranging from 34 nm to 70 nm. The setup being optimized for detecting low-energy light-charged particles in a veto detector embedded in a TPC active target. The preliminary results demonstrated a linear light response and energy resolutions comparable to those obtained with a standard sensor featuring an aluminized Mylar window. Further tests are currently underway, aimed at coupling the sensors with larger-area SiPMs ($6 \times 6\,\mathrm{mm}^2$), thin scintillators (1 mm thick) and PMMA light guide (to couple the scintillator with the SiPM and bringing the sensor far away from the TPC active region) in order to enhance light collection, lower the energy threshold and improve energy resolution.



2025 JINST 20 C08021

## Acknowledgments

Stefano Boscarino thanks the support by MUR-PNRR project SAMOTHRACE (Grant No. ECS00000022).

## References

[1] M.G. Pellegriti et al., *Measurement of $^8Li(\alpha,n)^{11}B$ cross section with ACTAR*, proposal to GANIL PAC **E864** (2022).

[2] S.K. Das et al., *New measurement of the $^8Li(\alpha,n)^{11}B$ reaction in a lower-energy region below the Coulomb barrier*, *Phys. Rev. C* **95** (2017) 055805.

[3] K.P. Artemov et al., *Effective method of study of α-cluster states*, *Sov. J. Nucl. Phys.* **52** (1990) 408.

[4] T. Roger et al., *Demonstrator Detection System for the Active Target and Time Projection Chamber (ACTAR TPC) project*, *Nucl. Instrum. Meth. A* **895** (2018) 126.

[5] Eljen EJ-212, https://eljentechnology.com/products/plastic-scintillators/.

[6] Eljen PMMA, https://eljentechnology.com/products/light-guides-and-acrylic-plastic.

[7] HAMAMATSU MPPC SiPM, https://www.hamamatsu.com/eu/en/product/optical-sensors/mppc.

[8] CAEN A7585DU SiPM Power Module, https://www.caen.it/products/a7585/.

[9] Nooelec HF109 LaNa ultra-low-noise HF amplifier, https://www.nooelec.com/store/downloads/dl/file/id/107/product/337/lana_hf_datasheet_revision_1.pdf.

[10] CAEN DT5743 digitizer, https://www.caen.it/products/dt5743/.

[11] J.F. Ziegler, M.D. Ziegler and J.P. Biersack, *SRIM — The stopping and range of ions in matter (2010)*, *Nucl. Instrum. Meth. B* **268** (2010) 1818.

[12] O.B. Tarasov et al., *$LISE^{++}_{cute}$, the latest generation of the $LISE^{++}$ package, to simulate rare isotope production with fragment-separators*, *Nucl. Instrum. Meth. B* **541** (2023) 4.

2025 JINST 20 C08021